Volume 140 | Number 14 | 21 July 2015 | Pages 4723–4905

Analyst

www.rsc.org/analyst

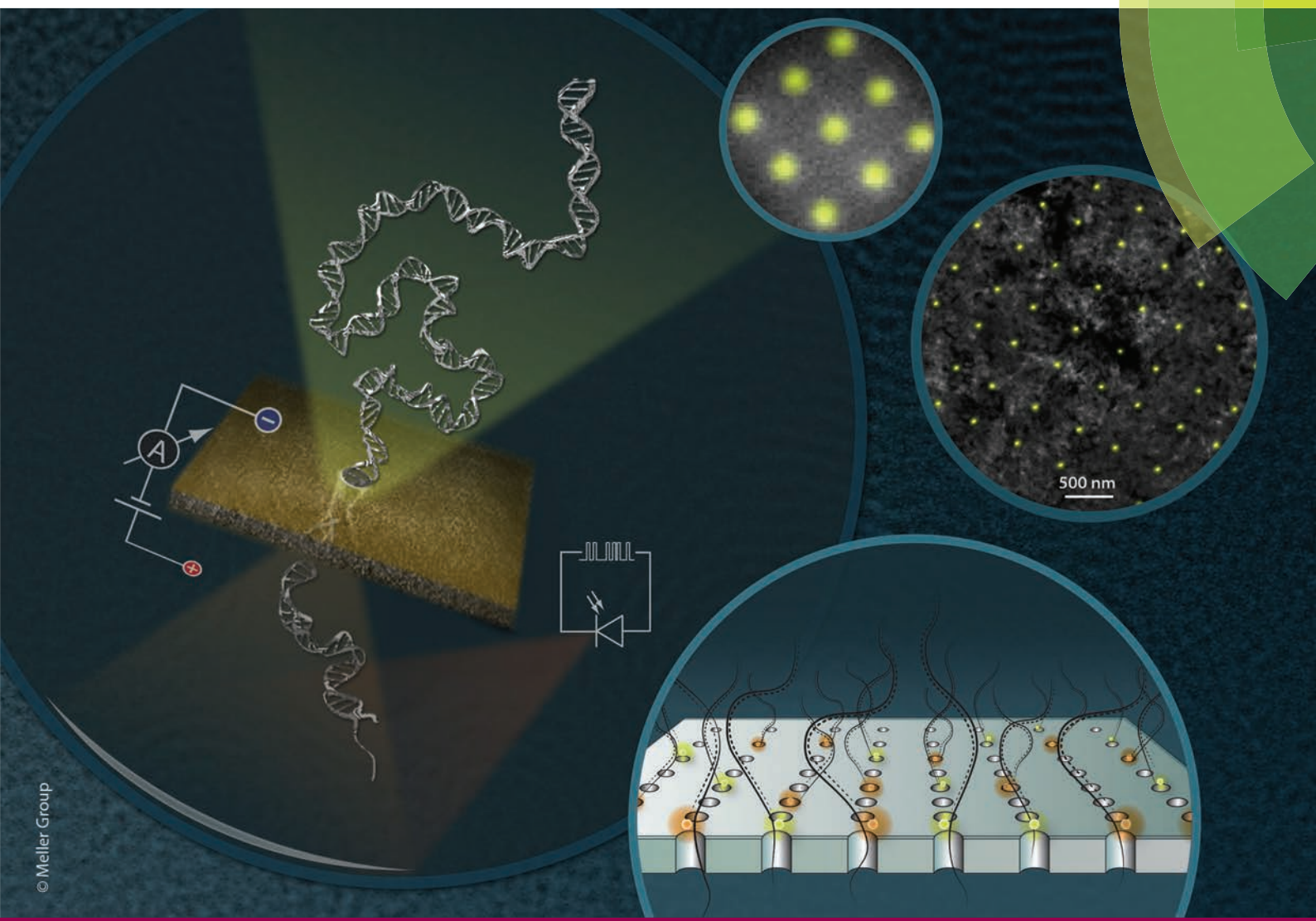

Themed issue: From nanopores to nanochannels

ISSN 0003-2654

ROYAL SOCIETY OF CHEMISTRY

MINIREVIEW
Tal Gilboa and Amit Meller
Optical sensing and analyte manipulation in solid-state nanopores

Analyst

MINIREVIEW

View Article Online
View Journal | View Issue

Cite this: *Analyst*, 2015, **140**, 4733

Optical sensing and analyte manipulation in solid-state nanopores

Tal Gilboa and Amit Meller*

The field of nanopore sensing has been gaining increasing attention. Much progress has been made towards biotechnological applications that involve electrical measurements of temporal changes in the ionic current flowing through the pore. But in many cases the electrical signal is restricted by the non-ideal noise components, limited throughput, and insufficient temporal or spatial resolutions. To address these limitations, high-sensitivity optical detection techniques that complement the electrical measurements have been developed. The optical techniques involve high-bandwidth, multicolor and high-throughput measurements. Here we review the recent advancements and developments that have been taking place in the field of optical sensing in solid-state nanopores. We describe the main optical methods used in this field involving total internal reflection and confocal microscopy in addition to sophisticated background suppression strategies. We further present the phenomenon of light induced analyte manipulation at the pore and the contribution of the optical sensing approach to possible nanopore sensing applications such as optical based DNA sequencing using nanopores.

Received 28th December 2014,
Accepted 3rd February 2015

DOI: 10.1039/c4an02388a

www.rsc.org/analyst

1. Introduction

Nanopores are an emerging class of single-molecule biosensors that has attracted increasing attention in the past decade due to three prominent features: (i) extremely high sensitivity,

Department of Biomedical Engineering, The Technion – Israel Institute of Technology, Haifa, Israel 32000. E-mail: ameller@bm.technion.ac.il

Tal Gilboa

Tal Gilboa is conducting her Ph.D. studies in the laboratory of prof. Amit Meller in the Department of Biomedical Engineering at the Technion–Israel Institute of Technology, Haifa, Israel. She completed her undergraduate degree in Biomedical Engineering at the Technion in 2012. Her research aims to improve optical sensing in nanopores and to implement multi-color detection, which will allow "barcoding" of DNA molecules. Her area of interest is in applying these tools in acute biomolecular diagnostic challenges, by developing a nanopore-based device for single-molecule DNA classification.

Amit Meller

Dr Amit Meller is a full professor in the Department of Biomedical Engineering and the Department of Biology at the Technion–Israel Institute of Technology, Haifa, Israel. He received his Ph.D. degree in Physics from Weizmann Institute, Israel in 1998. He then held a position as a Post-doctoral Fellow at Harvard University, commencing his work on Nanopore sensing. In 2000 Dr Meller was recruited to the Rowland Institute at Harvard University as a senior research fellow, where he established his single-molecule biophysics group. In 2006 Dr Meller joined the faculty of Boston University as an associate professor at the department of Biomedical Engineering and department of Physics. Dr Meller's current research interests include single-molecule sensing and single molecule biophysics, bio-optics, nano-sciences and nano-biotechnology.

with the ability to detect as low as a few atto-moles of DNA molecules,[1] (ii) versatility in terms of the different biomolecules they can probe, including DNA, RNA and proteins,[2,3] as well as their (iii) compact and miniature form factor, which lends itself to portable, point-of-care applications.[4] Solid-state nanopore sensors are composed of an ultrathin insulating membrane, typically only a few nanometers thick, in which a nanoscale pore or arrays containing multiple pores are formed.[5] The size of the nanopore can be tailored with subnanometer precision, to match the target analyte size.[6–8] Specifically, small nanopores in the size range of 2 nm to 20 nm, which are the focus of this review, have been broadly utilized to ensure single-file threading of individual biomolecules.[4,9] The thin membrane separates two liquid chambers containing either symmetrical or asymmetrical salt solution. To date, most studies have employed electrical ion-current measurements to detect and characterize biomolecule entry into, and passage through, the nanopores. Electrical sensing in nanopores has been utilized for a variety of sensing applications in biotechnology,[10] most prominently for direct, single-molecule nucleic acid sequencing,[11–18] probing of RNA structures,[15,19–21] probing of proteins[3,22,23] and genotyping of viral genes.[24,25]

In recent years, substantial progress has been made to improve the performance of nanopore sensors, particularly in their capacity to distinguish between fine macromolecular properties.[26] For example, the design of nanopore-based sequencing which can distinguish each of the four different nucleotides in a single-stranded DNA strand as it translocates through the pore has been a major goal in a number of studies. However, to date the development of real-life applications employing electrical sensing of solid-state nanopores has been stunted by three major factors:

(i) Noise and bandwidth: In a typical nanopore set up, the temporal resolution is limited to 1–10 μs due to the limited signal bandwidth of each element involved in the current measurements. Furthermore, the electrical signal is hindered by non-ideal ion current noise spectra, which involves low frequency ($1/f$) flicker noise as well as high frequency dielectric loss and capacitive noise, on top of the flat thermal noise (Johnson–Nyquist) and electronic shot noise.[27–30] These noise components are generally believed to be the key limiting factors of the technique's ability to resolve fine molecular features, as required in many sensing applications.

(ii) Throughput: The ability to process many biomolecules simultaneously is critical for numerous bio-technological applications, such as DNA sequencing and RNA expression analyses. Simultaneous multiplexed readouts from hundreds if not thousands of nanopores, without compromising the detection bandwidth and sensitivity, poses a central challenge in nanopore sensing design.[31]

(iii) Spatial information and spatial resolution: The typical nanopore channel is a few nanometers long. However, many molecular features (*i.e.*, a DNA nucleotide) are only a fraction of a nanometer in size, warranting development of strategies to further improve the nanopore spatial resolution.

A number of strategies have been proposed to address these limitations. In many cases, the improved approaches involve supplementation of the electrical ion measurement with additional electrical measurements. For example, integration of a pair of local nano-electrodes capable of injecting electrical current along the nanopore perimeter which is modulated by the biomolecule as it translocates through the pore[32] could provide the means to detect the fine molecular features of the translocating molecule. Similarly employment of an atomically thin substrate, such as graphene could improve the spatial resolution of the nanopore.[33–36]

Another approach, which is the focus of this review paper, involves complementation of the electrical sensing with high sensitivity optical detection. This approach is particularly powerful, in that it provides a measurement fundamentally independent of the electrical sensing that relies on photons rather than electrons. Importantly, optical sensing can be performed at the far-field, as photons (unlike electrons or ions) freely travel in the aqueous media surrounding the nanopores. This adjunctive feature opens up vast opportunities for light excitations and broad spectral emission, which will cause minimal interference with the local electrical measurement performed at the nanopore itself. Moreover, incorporation of optical sensing in nanopores introduces the benefits of a wealth of high-performance reagents, such as high-brightness fluorophores covering a broad spectral range, high-sensitivity sensors, including Avalanche Photo Diodes (APDs), Electron-Multiplying and Scientific CMOS CCD cameras and ultra-compact solid-state light sources spanning the near UV to the IR wavelength regimes and other components developed for single-molecule optical sensing.

This review first describes the most prominent optical methods employed for background noise suppression. Approaches designed to provide further background suppression are then detailed. The second section of this review is devoted to the use of Ca^{2+}-activated dyes, which are used as independent ion probes either in addition to, or in place of, direct ion current measurements. The probing fluorescence emitted by the Ca^{2+}-activated dyes yields signals highly localized to the pore vicinity and is less affected by charge fluctuations in the system, as compared to 'classical' ion current probing. The third section is dedicated to optical methods used to manipulate analytes at the nanopore. Specifically, we discuss methods to control the DNA or proteins translocation velocity by light. We then describe nanopore based optical DNA sequencing as an example for bio-sensing application that utilizes optical sensing. We finally end with a discussion and outlook for further improvements and developments in this field.

2. Optical approaches for single-molecule detection in solid-state nanopores

A principle common to essentially all optical-based single-molecule detection methods is the basic requirement to sup-

press the level of the background light to levels that permit detection of a *single fluorophore*. Here, we discuss two common methods that have been extensively used in single-molecule sensing, particularly for the detection of surface-immobilized biomolecules. Notably, adaptation of these methods for their combined use with solid-state nanopores has presented some non-trivial experimental challenges discussed here.

2.1. TIRF illumination

In total internal reflection fluorescence (TIRF), the excitation light is introduced from a higher refractive index medium to a lower refractive index medium at an angle slightly larger than the critical angle of incidence; thus the light is fully internally reflected at the interface of the two media.[37] Consequently, an exponentially decaying electromagnetic field (an evanescent field) is formed close to the interface, restricting the excitation of molecules to this narrow region and resulting in significantly less background light. Furthermore, since large surfaces can be excited using TIR, wide-field imaging devices (*i.e.*, EM-CCDs) can be used for parallel imaging of many molecules. Two main approaches have been developed for TIRF microscopy. In the prism-based approach, a small glass prism facilitates the introduction of the laser beam at an angle larger than the critical angle formed at the glass–water interface. The emitted light is imaged from the opposite side, by means of a long working distance objective. In the objective-based approach, a particularly high NA microscope objective (typically NA >1.40) is illuminated with a focused laser beam at its back focal plane at an off-axis point, creating a tilted collimated beam at the sample side. The tilting angle can be adjusted by simply controlling the offset distance of the laser beam at the objective back focal plane, to generate TIR illumination.

One of the challenges for adapting conventional TIRF approaches to the nanopore system is posed by the fact that the ultra-thin solid membrane where the TIR should be formed must be immersed in liquid buffer on both of its sides. While the nanopore membrane (typically silicon nitride) possesses a high index of refraction (about 2.0),[38] its ultra-thin thickness (~10 nm) renders it nearly transparent, and TIR cannot be formed in the common solid–liquid interface configuration. In 2010, Soni and coworkers proposed a simple solution to this issue by introducing asymmetric fluids at the *cis* and *trans* chambers.[39] Specifically, the index of refraction of the *trans* chamber solution (n_{trans}) was adjusted such that: $n_{cis} < n_{trans} < n_{glass}$, enabling generation of TIR at the SiN_x membrane, preventing light from progressing into the *cis* chamber where labeled biomolecules were introduced; overall, the background light emitted by molecules residing in the vicinity of the membrane, as well as scattered light from the buffer solution were reduced.

In addition, Soni and coworkers successfully synchronized the electrical signal with the optical signals for the first time, thereby providing the exact timing of each camera frame in sync with the ion current A/D sampling. In order to find the nanopore position on the SiN_x membrane, they took advantage of the fact that unlike the random behavior of background fluorescent spots, the fluorescence signal from the pore is stationary and lights up in synchrony with the electrical signal. Thus, the pixel corresponding to the pore location will, over time, accumulate the highest fluorescence intensity. Simple summation of all images captured during translocation of a fluorescently labeled molecule through the nanopore yields a clear peak, which corresponds to the pore position on the CCD. This procedure was utilized to trace the fluorescence intensity at the nanopore position over time. In this study, a ~400 bp DNA fragments each labeled randomly with 5 Alexa647 fluorophores were translocated through a 4 nm pore. The synchronous electrical and optical events (Fig. 1) clearly show that an optical signal can be obtained from the fast moving DNA molecules. Statistical analysis of hundreds of translocation events showed an optical signal to noise ratio >2.

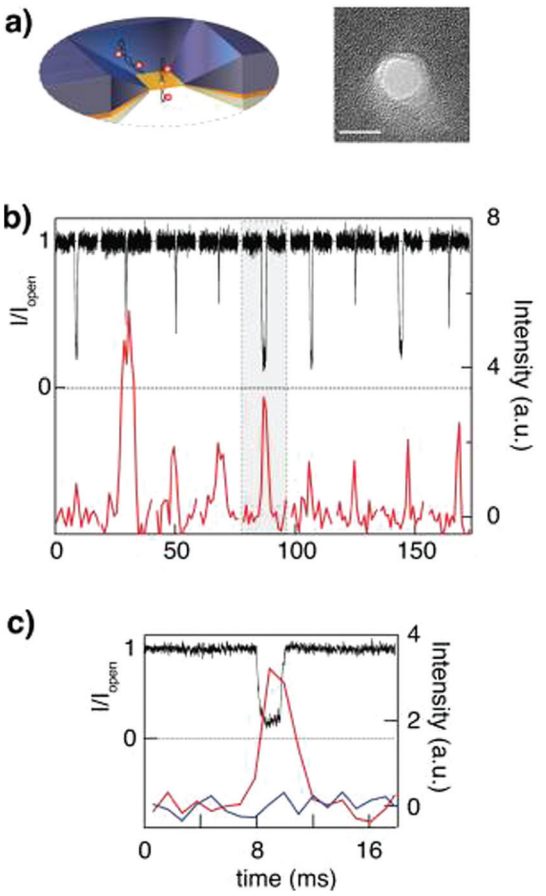

Fig. 1 Synchronous electrical and optical recording of dsDNA translocations through a solid-state nanopore. (a) Schematic illustration of labeled DNA fragments passing through a 4 nm nanopore (TEM image on the right). (b) A typical set of concatenated translocation events measured both optically (red lines) and electrically (black lines). (c) A magnified view of the highlighted event (gray background in b). Reprinted with permission from Soni *et al.*[39] Copyright 2010, AIP Publishing LLC.

2.2. Confocal illumination

In confocal imaging, the excitation laser beam is focused to a diffraction-limited spot and the emitted light at that spot is focused onto a spatial pinhole to reject out of focus light.[40] The light passing through the pinhole is then focused onto a point-like detector, such as an APD. High numerical aperture water immersion objectives are often used to minimize spherical aberrations. In the case of nanopore sensing, the pore must be precisely positioned, in three dimensions, at the confocal spot to maximize the detection efficiency.

Di Fiori and coworkers integrated confocal measurements with solid-state nanopore biosensing.[41] They focused an expanded 532 nm laser beam on the SiN_x membrane using a water immersion, 1.2 NA, 60× objective and used a closed-loop nano-positioner to position the nanochip at the confocal spot. Interestingly, *X*–*Y* scanning of the sample while registering the ion current passing through the pore revealed a sharp increase in the open pore current (i_O) when the laser spot overlapped with the nanopore position. This opto-electrical effect is due to light-induced surface charging of the SiN_x membrane, and is discussed in more detail in Section 3. Importantly, it enables fine alignment of the laser spot with the nanopore to sub-wavelength precision.

In the confocal setup described by Di Fiori and coworkers, the emitted light was focused onto a 100 μm pinhole, and then spectrally split, using a 640 nm dichroic mirror, onto two APDs, for two-color emission detection ('green' and 'red'). For data acquisition, the digital photon streams were fed to multichannel high-speed counters, and the analog ion current signal was digitized by an A/D card. In order to allow synchronization between the optical and electrical signals, the two cards shared the same 250 kHz sampling clock *via* a hardware connection, and were fully controlled by a custom program.

2.3. Background noise suppression strategies

The TIRF and confocal methods described above can suppress the background light originating from the bulk or out of focus regions of the sample. They, however, fail to suppress the background light emitted by the membrane itself, resulting from scattering, photoluminescence, or even weak fluorescence. This source of background is not negligible and was the focus of a few studies which aimed to minimize it.

The first approach involved modification of the SiN_x surface using atomic layer deposition (ALD) of various oxides.[42] dela Torre and coworkers showed that focused ion beam (FIB) fabricated nanopores and nanopore arrays in SiN_x can be coated with a TiO_2 layer *via* ALD.[31] The coating served a dual purpose: first, it reduced the nanopore size from roughly 25 nm down to 8 nm, and second, it decreased the surface photoluminescence. Specifically, the TiO_2 layer exhibited much lower photo-luminescence in the 580–660 nm range, when compared with the bare SiN_x. A proof of principle experiment using immobilized Q dots, showed that the TiO_2-coated membrane exhibits a three-fold reduction in the background noise level compared to a bare SiN_x membrane. They then performed optical detection of 1 kbp DNA molecules bound to streptavidin-coated quantum dots, using TiO_2-coated 6 × 6 nanopore arrays. When an external electrical field was applied across the membrane, the Qdots-DNA complexes were randomly drawn to the nanopores. The molecules that were captured in the pore became trapped inside the nanopore array due to the fact that the diameter of the Qdot was larger than the pore diameter. Upon application of a positive voltage, they observed distinct fluorescence signals in some of the pores, indicating Qdot–DNA conjugate lodging in each of the illuminated pores. Switching off the electric field resulted in disappearance of the fluorescence signal, due to escape of the Qdot–DNA from the pore.

Sawafta and coworkers utilized the beam of a commercial helium ion microscope (HIM) to achieve controllable reduction of the photoluminescence (PL) of SiN_x membranes and to produce nanopore arrays within the membrane.[43] They report a 20% reduction in membrane background noise level from that measured for its unmodified form. The HIM is characterized by a superior beam shape and imaging capabilities as compared with the dual beam FIB systems, allowing the direct fabrication of smaller nanopores, and avoidance of the need for additional post-fabrication processes, such as ALD.[44] The HIM has been used to fabricate larger nanopore arrays (20 × 20) with diameters of ~5 nm. Sawafta and coworkers used TIRF microscopy to image translocations of short ssDNA molecules labeled with 3 Cy3 fluorophores; the video was collected while applying 1 V across the membrane (Fig. 2). Transient increases in fluorescence at the location of the pores were observed, which could have resulted from translocation of the ssDNA molecules through the pores or from free diffusion of a fluorophore into the focal volume of the microscope. Analysis of the event rate showed that the vast majority of the fluorescence spikes measured in the nanopore array corresponded to translocation events or stochastic interactions with the sensing region. In the future, simultaneous measurement of the optical and electrical signals may provide the key to differentiating between true translocations through the pores and other interactions that do not involve translocation.

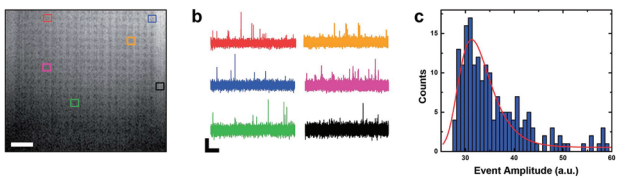

Fig. 2 Parallel optical detection of Cy3 labeled DNA molecules translocating through nanopore array. (a) Fluorescence image of a 20 × 20 nanopores array fabricated in a SiN_x membrane. The image is an average of 100 video frames after contrast adjustment. Scale bar is 2.5 μm. (b) Optical measurements recorded simultaneously from 5 different pores within the array (each outlined in corresponding color) and from a region on the membrane proximal to the array (black lines). Scale bar is 0.5 s (horizontal) and 30 a.u. (vertical). (c) Amplitude histogram of 191 optical events measured at the locations of individual nanopores within the array and a log normal fit to the data (red line). Adapted from Sawafta *et al.*[43] with permission of The Royal Society of Chemistry.

PL in supported SiN_x films has been extensively studied and characterized.[45,46] However, much less is known about PL behavior in freestanding, ultrathin SiN_x membranes, which are the most-commonly used substrates for solid-state nanopore measurements. Understanding PL properties is a crucial step toward the possibility of low SNR optical measurements in solid-state nanopores. Assad and coworkers investigated the effect of controlled focused e-beam irradiation on the optical properties of nanopores made in SiN_x membranes.[47] They illuminated ultrathin SiN_x membranes, immersed in a 1 M KCl buffer, using blue (488 nm), green (532 nm) and red (640 nm) lasers and measured the emitted PL spectra with a spectrometer. Their results showed that, unlike the red laser that induced low PL, the blue and green excitations produced a broad PL emission band, which substantially overlapped with the emission spectra of common high brightness fluorophores and substantially reduced the SNR (Fig. 3a). This can explain why the excitation was restricted to red laser excitation and far-red dyes in all previous optical experiments performed using nanopores.[16] The group then repeated the measurements at three different regions on the same silicon nitride membrane: a thick region (60 nm), a thin region (15 nm) and a thin region after an exposure to a high e-beam dose, which resulted in nanopore formation (Fig. 3b). The shapes of the three spectra measured for the three regions were mostly similar, however, membrane thinning led to a reduction in PL. Electron beam irradiation resulted in an additional reduction by a factor of 2, with respect to the unexposed 15 nm thick area. These results propose two factors underlying reduced PL: thinning down of the silicon nitride and its exposure to a high-dose electron beam.

In order to understand the mechanism through which e-beam exposure affects the PL intensity and spectra, they compared six thin (15 nm thick) regions on the same SiN_x membrane that had been irradiated with different e-beam doses. Upon excitation with a 488 nm laser, the PL intensity dropped from an initial level of 670 ± 30 counts per millisecond per milliwatt (Cpms mW^{-1}) with no e-beam dose, to less than 330 ± 14 Cpms mW^{-1} when the e-beam dose reached 56×10^6 electron nm^{-2}, yet remained roughly stagnant for even larger e-beam dosages. The obtained data fit nicely to an exponential function with an offset baseline, which indicates that there is an additional factor aside from e-beam irradiation controlling the membrane PL. Exposure of thin and thick membrane regions to e-beam for an extended period of time resulted in similar PL levels, which implies that this PL contribution does not arise from the bulk material.[48,49] Following the observations presented above, Assad *et al.* suggested that highly localized e-beam irradiation of SiN_x during the drilling process of solid-state nanopores induces substantial alterations to the membrane's material properties, resulting in a measurable reduction of the PL intensity and in a blue shift of its spectrum.[47]

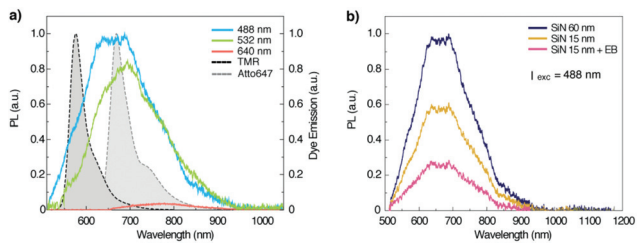

Fig. 3 Photoluminescence spectra of ultrathin SiN_x membranes suspended in 1 M Kcl buffer. (a) Spectra measured under illumination of blue (488 nm), green (532 nm), or red (640 nm) lasers. Data is normalized by the incoming lasers intensities to permit comparison. Emission spectra of two common single-molecule fluorophores: TMR and Atto647. (b) Spectra measured at three different regions on the same silicon nitride membrane excited by 488 nm laser: a thick region (60 nm) a thin region (15 nm) and a thin region after an exposure to a high e-beam dose, forming a nanopore. Adapted with permission from Assad *et al.*[47] Copyright 2014 American Chemical Society.

3. Optical detection in solid-state nanopores with Ca^{2+}-activated dyes

Ca^{2+}-activated dyes are organic molecules that become fluorescent upon binding to Ca^{2+} ions.[50] They are commonly used in neuroscience research to monitor neural activity and Ca^{2+} signaling. In nanopore experiments, Ca^{2+}-activated dyes can serve as an indicator of the local Ca^{2+} ions concentration near the pore, thus substituting direct ion measurement using the $AgCl^-$ electrodes with optical signals. This offers a number of potential benefits towards label-free sensing of analytes in nanopores. First, such dyes can be used to detect the simultaneous ion current flow through multiple pores, without the need to equip each and every pore with its own set of electrodes that must be electrically isolated from one another. Second, due to the nature of the chemical gradient of ions near the pore, the optical signals are localized to the pore region, and are less affected by ion concentration fluctuations at distances from the pore, as compared to the electrical probes. In principle, this may lead to superior noise characteristics.

Heron and co-workers used Ca^{2+}-activated dyes in protein nanopores to probe the stochastic on/off binding kinetics of cyclodextrin to the alpha hemolysin pore by monitoring the fluorescence signal arising from each pore.[51] More recently, two groups independently presented the ability to use Ca^{2+}-activated dyes for optic detection of unlabeled DNA molecules in solid-state nanopores,[52,53] employing higher bandwidth measurements than the previous study. The principle behind the method is to create a Ca^{2+} ion gradient across the pore by injecting high Ca^{2+} concentration in the lower chamber (*trans*) and no calcium in the upper chamber (*cis*). Utilizing numerical simulations, Anderson and co-workers showed that the Ca^{2+} ion distribution around the nanopore can be finely tuned within the pore vicinity by varying the voltage or the Ca^{2+} bulk concentration.[53,54] Under these conditions, the addition of low concentrations of a Ca^{2+} indicator dye to the *cis* side results in a highly localized and voltage-tunable fluorescent spot

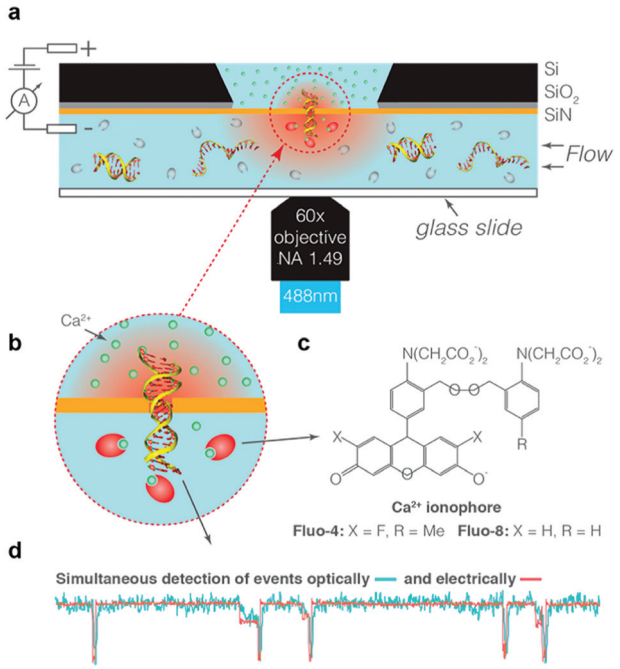

Fig. 4 Chemo optical sensing in solid-state nanopores using Ca^{2+} gradient and calcium activated dyes. (a) Schematic of the measurement set up. The ion current flowing through the pore is probed electrically using Ag/AgCl electrodes and optically using *epi* illumination for the excitation of the Ca^{2+} indicator dyes and EM-CCD camera for the fluorescence detection. (b) Zoom in on the nanopore area. A gradient of Ca^{2+} ions is created across the pore by using high Ca^{2+} concentration in the upper chamber (*trans*) and no calcium in the bottom chamber (*cis*). The addition of Ca^{2+} indicator dye to the *cis* side results in a highly localized and voltage-tunable fluorescent spot in the vicinity of the pore. (c) The chemical structure of the calcium activated dyes. (d) Simultaneous electrical and optical detection of translocation events. The entry and passage of the biopolymer through the pore results in a drop in the ionic current (red trace) and thus a decrease in the fluorescence intensity (blue trace). Adapted with permission from Ivankin *et al.*[52] Copyright 2014 American Chemical Society.

immediately outside the nanopore. When a DNA molecule translocates through the pore, it partially blocks the Ca^{2+} flow through the pore, thereby creating an immediate drop in the Ca^{2+} flow and a corresponding drop in the optical signal (Fig. 4).

Both groups presented the ability to use this method for simultaneous detection of DNA translocation events through multiple pores. Ivankin and co-workers employed *epi*-illumination for the excitation of the Ca^{2+}-activated dyes and an EM-CCD camera for fluorescence detection. They translocated ~150 nt-long ssDNA molecules through three nanopores (2 nm diameter) and simultaneously detected events occurring through the pores. These authors observed a substantial photo-bleaching rate, presumably due to the use of *epi*-fluorescence illumination, and employed a constant flow of fresh dyes. Anderson and co-workers used TIRF illumination, which permitted the use of much lower laser excitation per unit area, while allowing a somewhat faster frame rate capture. They demonstrated the feasibility of multipore imaging on a 3 × 3 nanopore array (4 nm diameter). Of the nine nanopores simultaneously probed in this measurement, four displayed DNA translocation events (8 kbp), one became partially blocked after 20 seconds, and the other pores remained open.

In addition to the TIRF measurements, Anderson and co-workers developed a method to couple the ionic current to photon-by-photon counting of the fluorescence signal emanating from the Ca^{2+}-sensitive dyes and demonstrated label-free optical detection of biopolymer translocation through solid-state nanopores using confocal microscopy.[53] This provided for higher photon count rates while utilizing pure digital photon counting. They illuminated the nanopore with a focused laser beam, counted individual emitted photons, using APDs, and simultaneously recorded both electrical and optical open pore currents. In order to compare the electrical and optical noise characteristics, they estimated the power spectra for both signals (Fig. 5a,b). The resulting electrical spectrum displayed the typical noise characteristics discussed above. In contrast, the corresponding optical spectrum was virtually flat from 5 Hz to 100 kHz, and specifically, no spurious noise was observed. Anderson *et al.* suggested that the observed difference in the noise profile stems from the fact that, unlike the electrical signal, which is measured using electrodes positioned hundreds of micrometers from the pore, the optical signal is generated in the immediate vicinity of the pore, thus involving only local sources of noise (*i.e.*, mainly thermal noise and shot noise). Furthermore, photon arrivals are an inherently digital stream of information, whereas the electrical ion current is an analog signal, subject to sampling error and noise. They further measured and calculated the SNR for the APD counts for three average fluorescence emission intensities (1.3, 4.0, and 9.8 Mcps) and demonstrated substantial growth of the SNR with the average count rate (which can be tuned *via* the activated fluorophore concentration and excitation intensity) (Fig. 5c). Further improvement in the emission count rates will potentially allow researchers to obtain even higher bandwidths than those available today in typical electrical nanopore measurements.

4. Light-driven manipulation of analytes in solid-state nanopores

4.1. Controlling the analytes' translocation speed

Both the electrical and optical signals associated with nanopore sensors are constrained by their corresponding noise levels and the underlying noise spectra. To understand the various trade-offs associated with the technique, it is constructive to define the signal-to-noise ratio (SNR) as:

$$\mathrm{SNR(BW)} = \frac{\Delta i}{i_{\mathrm{RMS}}(\mathrm{BW})} \quad (1)$$

where Δi is the minimal signal (electrical or optical) amplitude required to make a confident call between two states, and i_{RMS} is the bandwidth (BW)-dependent root mean square (rms)

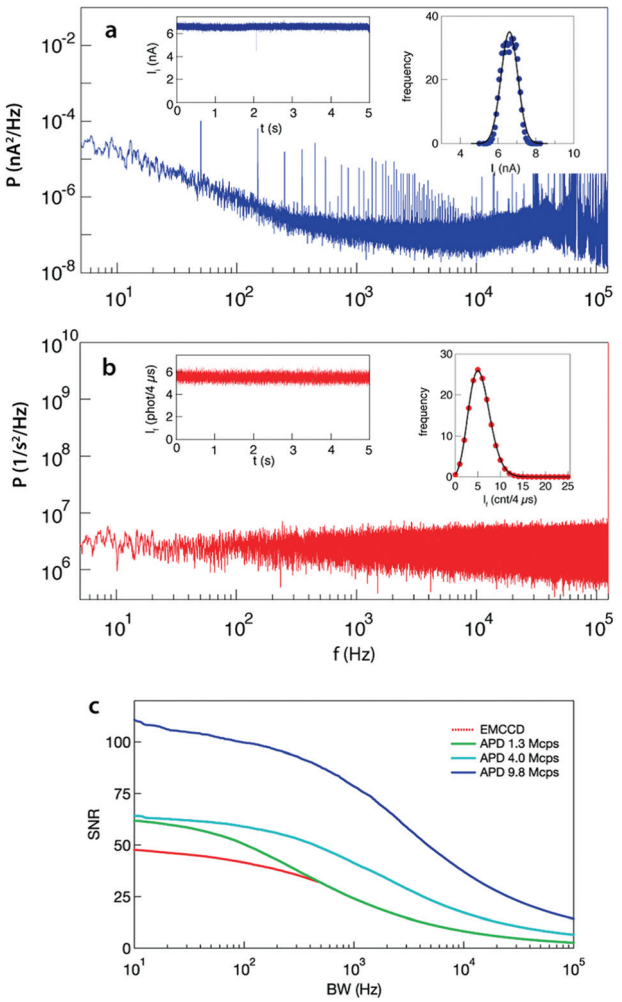

Fig. 5 Electrical and optical noise spectra. (a) The electrical noise exhibits low frequency 1/*f* noise as well as high ~f^2 capacitance noise on top of white thermal noise and shot noise. (Inset) The electrical current histogram fit with a Gaussian distribution (mean = 6.57 ± 0.03 nA, width = 0.77 ± 0.07, χ^2 = 2.25). (b) The optical noise spectra, virtually flat from 5 to 100 kHz. (Inset) The optical current histogram fit with a Poisson distribution (mean = 5.55 ± 0.01 cnts/4 μs, χ^2 = 0.96). (C) SNR for the optical signals as a function of the bandwidth evaluated using: $\mathrm{SNR} = I_{\mathrm{avg}}/I_{\mathrm{RMS}}(\mathrm{BW})$, $I_{\mathrm{RMS}}(\mathrm{BW}) = \sqrt{\int^{\mathrm{BW}} \mathrm{PSD}df}$ showing positive function of the total number of counts. Adapted with permission from Anderson *et al.*[53] Copyright 2014 American Chemical Society.

noise level. A confident nanopore measurement is only possible when SNR(BW) > ε, where ε, is a number greater than unity. For example, in a nanopore sequencing application, Δi would be the smallest ion current or photon count required to discriminate between the two closest levels associated with two different nucleotides, and i_{RMS} is the calculated rms value of the mean signal level at the bandwidth corresponding to the same measurement. Importantly, as the bandwidth is increased, the i_{RMS} also increases, while the SNR is reduced. Generally, in single-molecule measurements, particularly in nanopore measurements, it is crucial to make the distinction between the instrument bandwidth $\mathrm{BW_I}$ and the measurement bandwidth $\mathrm{BW_M}$. The instrument bandwidth simply reflects the maximal frequency that can be measured by the instrumentation being used before it is attenuated by its internal components. In contrast, the measurement bandwidth is an application-specific parameter defined by the inverse of the minimum amount of time that the signal Δi is integrated. For example, if a DNA strand translocates through the nanopore at a maximal velocity $\nu_{\max}$ and the base-to-base distance in the DNA is a, $\mathrm{BW_M} = \nu_{\max}/a$. Clearly, two conditions must be met to obtain a reliable measurement. First, $\mathrm{BW_M} < \mathrm{BW_I}$, otherwise the obtained signal will be biased by the instrumentation. Second, $\mathrm{SNR}(\mathrm{BW_M}) > \varepsilon$ to ensure a reliable readout not masked by noise. Therefore, the ability to control and manipulate $\nu_{\max}$, with subsequent control of the measurement bandwidth, in a way that does not impact the signal (Δi), is of pivotal importance in nanopore sensing.

One way by which $\nu_{\max}$ can be controlled is by coupling a molecular ratcheting enzyme to the nanopore (for example a DNA polymerase), to regulate the speed of the DNA strand translocation through the nanopore.[55] This idea was successfully adopted to develop protein pore-based DNA sequencing methods. There are, however, limitations on the use of molecular motors as a means to regulate strand translocation velocity, which motivated the development of purely physical approaches for controlling $\nu_{\max}$. Among the various approaches that were proposed for controlling $\nu_{\max}$, we focus on those which take advantage of light-induced phenomena. Specifically, theoretical studies showed that a controlled electro-osmotic flow in the direction opposing the DNA translocation, could be an efficient and general means of regulating $\nu_{\max}$.

Recently, Di Fiori and coworkers showed that a low-power visible laser beam can be used to directly enhance the surface charge of a solid-state nanopore. This, in turn, resulted in modulation of the associated electro-osmotic flow, which allowed them to control the translocation speed of DNA as well as protein molecules through the nanopore.[41] In this work, a low-power green laser (532 nm) was focused, using confocal microscopy, on a silicon nitride membrane containing a single nanopore. As the membrane was scanned with the laser, a substantial increase in the open pore current was observed once the laser spot overlapped with the nanopore location (Fig. 6). Di Fiori *et al.* reported a linear dependence of the change in the pore current at varying laser intensities (dI/dP), on nanopore diameter. This observation indicated that the photoconductance-induced charge enhancement is a surface rather than a volumetric phenomenon. They hypothesized that the laser illumination on the nanopore creates an increased surface charge density on the nanopore walls. The surface charges induce a diffuse double layer containing an excess of oppositely charged ions, of a thickness comparable to the Debye screening length k^{-1}. The electrical double layer creates a local imbalance of counter ions within k^{-1}, which drags water molecules with its motion, creating an electroosmotic flow (EOF) that, in turn, results in an increase in the open pore current.[56]

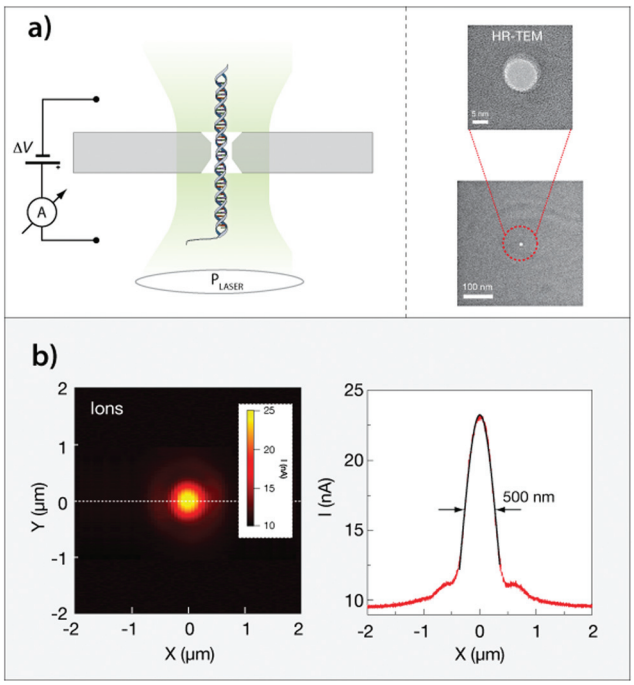

Fig. 6 The optoelectric effect in solid-state nanopores. (a) The green laser is focused on the pore using confocal illumination and the electrical current is measured using a pair of Ag/AgCl electrodes. TEM image on a 10 nm pore on the right. (b) Surface plot of the current measured while a 4 × 4 μm^2 region on the membrane is scanned using a focused 10 mW green laser beam at 1 μm s^{-1}. When the laser bean overlaps the nanopore a significant current enhancement is observed. Reprinted with permission from Macmillan Publishers Ltd: Nature Nanotechnology, Di Fiori *et al.*[41] copyright 2013.

Furthermore, the translocation speed of the biopolymers passing through the pore was dramatically reduced when the laser was focused on the pore. This phenomenon is in line with light-induced surface charging and was explained by the increase in the EOF in a direction opposite that of the DNA velocity in the pore. Thus, the laser light can be used to dynamically modulate the DNA translocation speed and hence, the translocation time of the DNA.

Further insight into the photoconductive effect was obtained by a simple model constructed to quantify this phenomenon. The ability of the nanopore surface to acquire charge when illuminated by the laser light, was defined empirically as the photoreactivity, γ (in units of C m^{-2} W^{-1}). For sufficiently low laser power, the surface charge density (σ) is assumed to grow linearly with the laser intensity (P) such that: $\sigma = \gamma P$. The reactivity,γ, is a specific property of each nanopore and depends on its fabrication process. Importantly, γ can be directly determined for each nanopore from the dependence of the open pore current on the laser intensity $i_O(P)$. Translocation experiments using different DNA lengths and different nanopore diameters were all shown to collapse on a single universal curve describing the retardation factor (the magnitude of slowing down upon exposure to light with respect to the no- light conditions) as a function of the nanopore surface charge density calculated using each pore's photoreactivity value.

Di Fiori's results show that the DNA and protein translocation speed through a photoreactive nanopore can be controlled by either the laser intensity or by the pore photoreactivity (Fig. 7). The latter was found to directly correlate with the electron beam dosage: pores exposed to a high electron beam dose had much higher photoreactivity in comparison with those that were drilled with a low electron beam dose. It was proposed that the high dose of electrons reduces the N/Si ratio around the pore and when this ratio is sufficiently low, the visible light can excite electrons from the ground state across the bandgap, trapping them in Si dangling bonds.[57,58] Eventually, trapped electrons recombine with holes, but a high density of arriving photons can maintain a steady state of negatively charged Si dangling bonds, creating a net surface charge density.

4.2. Conductivity manipulation

Manipulation of the ionic conduction in solid-state nanopores can be achieved by variation in the local temperature. In 2005, Keyser *et al.* showed that the temperature of the liquid in a solid-state device can be increased using a focused high-power infrared laser beam.[59] They scanned the pore, measured the ionic current, and calculated the local temperature by means of the linear temperature dependence of KCl conductivity. However, due to the low absorption coefficient of the aqueous buffer medium, this technique was suitable only for high intensity lasers (a few Watts).

Recently, Jonsson *et al.* presented an improved approach to profiling low-intensity optical field distribution at subdiffraction-limited resolutions.[60] In this study, a single plasmonic gold bowtie nanoantenna was fabricated on top of a thin silicon nitride membrane and a 10 nm nanopore was drilled at the center of the structure (Fig. 8). Finite difference time domain (FDTD) simulations were used to guide the design of the bowtie antennas so that their plasmon resonance matched the near IR laser wavelength (785 nm) when excited with light polarized along the long side of the structure. Each bowtie consisted of two equilateral gold triangles, separated by a 10 nm gap, with a thickness of 30 nm and a length of 60 nm from the tip to the opposite flat side of the triangle.

The nanoantenna can be used to focus an electromagnetic field to the sub-diffraction gap region between the two gold triangles, where the optical field intensity is amplified. The plasmonic antenna acted like a nanodetector that converts optical intensity variations into temperature variations that, in return, change the measured nanopore's ionic conductance (G), according to (in KCl solution):

$$G = \left(\frac{4h}{\pi d^2} + \frac{1}{d}\right)\mu c_{\mathrm{KCl}} e \qquad \mu = \mu_{\mathrm{K}} + \mu_{\mathrm{Cl}} \propto 1/\eta \qquad (2)$$

where h is the membrane effective thickness, d is the pore diameter, μ is the total ion mobilities, which is inversely depen-

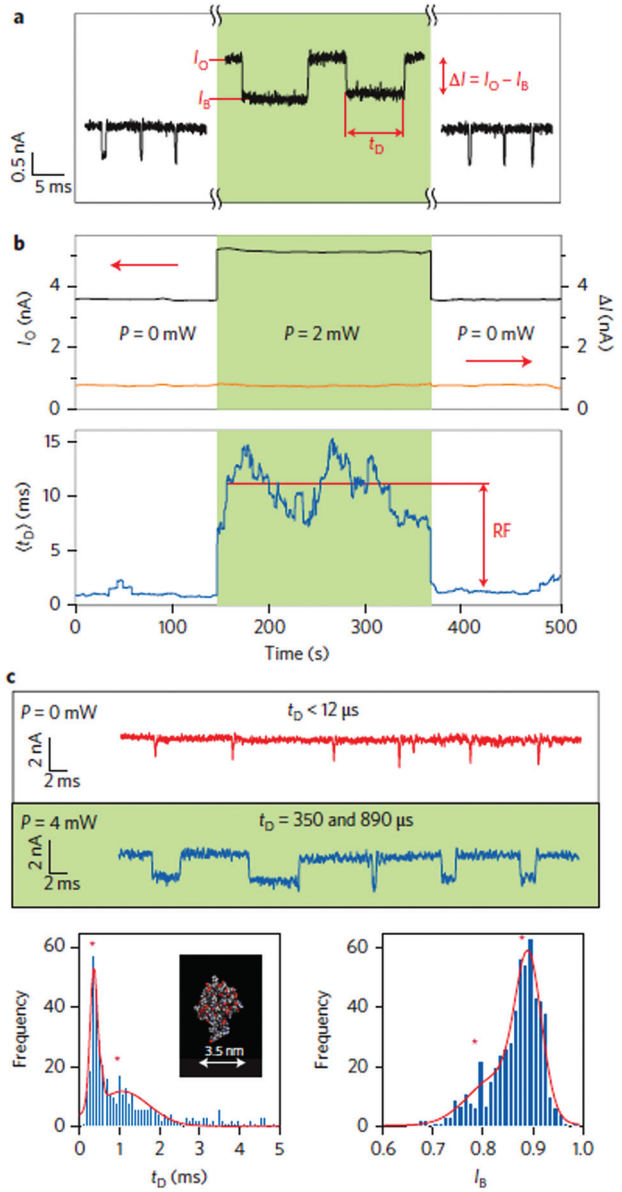

Fig. 7 Slowing down the translocation speed of DNA molecules and proteins using light. (a) Translocation events of 10 kbp DNA molecules in a 5.4 nm nanopore. Once a 2 mW laser beam (pre-aligned with the nanopore) is switched on, the open pore current (I_O), the blockade current (I_B) and translocation time (t_D) increase. The blocked current amplitude (ΔI) remains constant. (b) Traces of the open-pore current (I_O), blocked current amplitude (ΔI) and the mean translocation time ($<t_D>$) as a function of time. $<t_D>$ represent a running average over 150 translocation events, initialized at the moment the laser is switched on/off. (c) Translocation events of ubiquitin, a small-molecular-weight protein, in its native state in a 5 nm pore. Two orders of magnitude increase in the traslocation time is observed under illumination of 4 mW focused lased (blue line) in comparison with the translocations recorded before switching on the laser (red line). Histograms of the translocation time (t_D) and fractional blockade current (I_B) calculated using more than 500 events. The results show two prominent timescales for ubiquitin translocation time (340 ± 5 ms and 890 ± 70 ms), as well as two peaks in the blockade currents (0.88 and 0.78), approximated by a sum of two Gaussians (red lines). Inset: Crystallographic structure of wild-type human ubiquitin (PDB 1d3z). Reprinted with permission from Macmillan Publishers Ltd: Nature Nanotechnology, Di Fiori *et al.*[41] Copyright 2013.

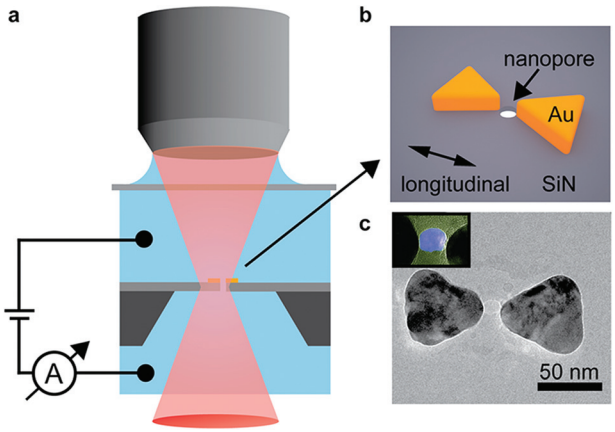

Fig. 8 The principle of plasmonic nanopore optical profiling. (a) Schematic illustration of the measurement set up. A 785 nm laser was focused into a flow cell, the position of the flow cell was controlled using a piezo stage to allow three dimensional scanning. The variations in the optical intensity within a focal zone caused temperature changes in the nanoplasmonic structure that were measured electrically through changes in the ionic conductance. (b) Three dimensional schematic illustration of the plasmonic bowtie nanoantenna with a nanopore in the gap. (c) TEM image of the plasmonic nanopore showing the plasmonic antenna consisting of two gold nanotriangles separated by a 10 nm gap in which a 10 nm nanopore was drilled. Adapted with permission from Jonsson *et al.*[60] Copyright 2013 American Chemical Society.

dent on the buffer viscosity η, c_{KCl} is the ion molar concentration and e is the elementary charge. Aqueous buffer viscosity empirically inversely depends, to a good approximation, on the temperature, expressed in degrees Celsius.[61] Thus, we can see that: $G \propto T(^{\circ}C)$. Unlike the approach presented by Keyser *et al.*, which was based on light absorption by the buffer, this method is based on local light absorption by the nanopore itself, through excitation of plasmons in the nanoantenna. In consequence, a greater heating can be obtained and signals are nearly 2 orders of magnitude higher compared to those obtained using direct heating.

In a follow up study, Nicoli and coworkers demonstrated label-free detection of DNA molecules using the same solid-state plasmonic nanopores, and explored the effects of plasmon excitation on the translocation parameters.[62] They added 48.5 kilo basepair dsDNA molecules in 1 M KCl buffer to one of the chambers, applied a 100 mV potential across the membrane and measured the ionic current with and without plasmonic excitation. Their results showed that both the open pore current and the conductance blockade increased upon laser excitation. However, the relative conductance blockades ($\Delta G/G$) decreased slightly with increasing laser power, likely due to other effects beside heating, such as light-induced changes in the surface charge density at the pore wall.[41] Interestingly, they did not observe significant changes in the translocation time upon plasmonic excitation. This may result from the fact that plasmonic heating is a highly local phenomenon, or from a balance between the competing effects of increased temperature and light-induced surface charging

of the nanopore. Similar results were obtained in 2 M LiCl buffer.

4.3. Events rate manipulation

In addition to conductance manipulations, Nicoli and co-workers showed that the plasmonic system could be used as a tool for controllable and reversible manipulation of the events rate in LiCl buffers. In the experiments performed, the event rate in 2 M LiCl buffer was measured under different laser intensities. The 2 M LiCl buffer has a conductivity similar to 1 M KCL, with the ability to provide for significantly lower translocation velocities but at the expense of low event rates. Upon longitudinal excitation with a 2 mW laser, they observed an order of magnitude enhancement in the event rate excitation. A ~30% of the enhancement in the longitudinal mode was also observed in the transverse mode. The measurements were repeated using different plasmonic nanopore chips and polarizations and the relative increase in open pore current under laser illumination ($\delta I/I$, where δI is the difference between the open pore current with and without laser illumination) was calculated. Interestingly, all the results collapsed to display a linear dependence of the event rate on $\delta I/I$. This result, in addition to the insensitivity to the other experimental conditions (specifically to polarization), indicates that the event rate enhancement is related to the strong and local thermal gradients caused by plasmon-induced heating. To explain this, Nicoli *et al.* proposed that negative thermophoresis (in which molecules move from cold to warm regions) facilitates capture of the DNA molecules by moving them toward the warmer nanopore.[63,64] Unlike LiCl, which is known to result in negative thermophoresis, KCl induces positive thermophoresis and, indeed, the rate enhancement effect was not observed for DNA translocations in KCl buffer.

5. Applications – next-generation DNA sequencing and beyond

The high demand for low-cost and ultra-fast sequencing technologies has driven the development of multiple, novel single-molecule methods.[65] Among them, nanopore based DNA sequencing is widely considered to be a promising next-generation sequencing platform.[11,66] As of the writing of this paper, protein pores (*i.e.*, MspA) have already been shown to effectively sequence DNA strands.[12,14,55] This was achieved by reducing the translocation speed of the DNA strands by coupling them to ratcheting enzymes. Two primary challenges for the method still remain: First, improving the base calling accuracy and its ability to read any arbitrary sequence including long repeats. Second, realizing a drastic boost in the overall throughput of nanopore sequencing by simultaneous readout from hundreds if not thousands of nanopore. These may potentially be addressed by employing optical-based nanopore techniques with high-density nanopore arrays.[31,43]

Soni *et al.* first introduced an optical-based nanopore sequencing approach that involves two steps.[17] First, a sample preparation in which the DNA is converted to an expanded form, followed by hybridization of fluorescently-labeled probes to each expanded base. Second, the fluorescent markers are optically detected, using an array of nanopores and TIRF illumination (Fig. 9). The main advantage of the method is that it simplifies the readout procedure to involve only four different-colored fluorophores. In contrast, the current electrical-based nanopore sequencing method involves a readout of 3 (or 4) nucleotides groups, which theoretically, require discrimination among $4^3 = 64$ different current levels, although sophisticated algorithms can be used to reduce this number by exploiting the fact that DNA is ratcheted through the pore in discrete single-nucleotides steps and that each base is read 3 (or 4) times in a different sequence context.[67,68] The optical approach in contrast, does not involve ratcheting enzymes and thus can theoretically achieve a higher strand loading efficiency and higher sequencing speed.

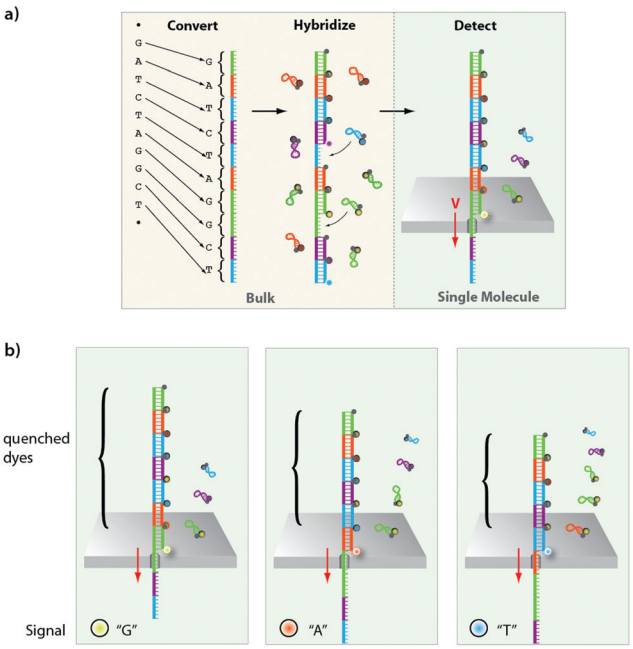

Fig. 9 Schematic Illustration of the optical sequencing method. Each base is converted to an extended sequence that is hybridized to a fluorophore–quencher beacon, where each base is represented by a different fluorophore color. The DNA/beacon complex in then threaded through a nanopore and the color barcode is detected optically. Each released beacon is automatically closed, quenching its own fluorescence while diffusing away from the vicinity of the pore.

These advantages, however, come at the price of an elaborate DNA preparation step, in which each of the four different nucleotides in the DNA strand is substituted with its own unique code oligonucleotide (typically ~15 nucleotide long). The substitution (or "DNA conversion") process involves cyclic ligations of the correct code oligonucleotide and digestion of the original bases. This off-line process can be simultaneously performed with a vast number of DNA molecules and does not require enzyme immobilization or an amplification step. After converting the DNA molecules, four different molecular

beacons complementary to the four possible oligonucleotide codes are specifically hybridized to the converted DNA. Each of the four beacons contains a different color fluorophore on its 5′ end and a quencher on its 3′ end. The broad-spectrum quencher molecule quenches both fluorophores and the four different color fluorophores make it possible to distinguish between them.

The converted DNA strands and hybridized beacons are electrophoretically threaded through an array of nanopores, designed to bear a diameter that allows only one strand to translocate through it. The pores are illuminated with a laser source in TIR mode and optically monitored using EMCCD. When the DNA molecule enters the pore, the marked beacons are stripped off one at a time, creating a distinct burst of fluorescence. Each released beacon is automatically closed, quenching its own fluorescence while diffusing away from the vicinity of the pore (Fig. 9, lower panel). The stripping process slows down the translocation speed of the DNA to approximately a few ms per unzipping event. This unzipping time can be tuned by the voltage applied.

McNally and coworkers performed proof of concept experiments to validate this new sequencing method.[16] In order to use larger pores than the ones needed for the unzipping process (~2 nm), they covalently attached a "bulky" group (*e.g.*, a protein or a nanoparticle) to the molecular beacons, which effectively increased the molecular cross section of the complex to 5–7 nm, enabling use of 3–5 nm pores. In this study, each of the four possible nucleotides was represented by two successive beacons (or "bits"), allowing for use of two colors only. To test the ability to observe the 2 bit signal, they prepared two samples: a 1 bit sample in which they attached an avidin (4 × 5 × 6 nm) to a biotinylated molecular beacon containing a fluorophore-quencher pair, in addition to a similar beacon without a fluorophore, both hybridized to a target ssDNA, and a 2 bit sample with a similar complex but with two beacons containing a fluorophore–quencher pair. The optical signals clearly showed one and two-photon bursts for the 1-bit and 2-bit samples, respectively.

Next, they performed two-color unzipping experiments with two high quantum yield fluorophores A647 (ATTO647N) and A680 (ATTO680), simultaneously excited by the same red laser. The optical emission was split into two channels using a dichroic mirror and simultaneously imaged by a single EM-CCD camera. Due to the overlap between the emission spectra of the two fluorophores, they performed calibration experiments using 1-bit complexes labeled either with A647 or A680. The ratio of the fluorescence intensities in Channel 2 *versus* Channel 1 was 0.2 ± 0.06 for the A647 sample and 0.4 ± 0.05 for the A680 sample. The ratios for the accumulation of all the events were 0.2 and 0.4 for the A647- and A680-labeled sample, respectively. The control measurements showed that the color ratio can be used in order to determine the identity of individual fluorophores. The error in the determination of each of the two fluorophores was calculated from the overlap area between the distributions, yielding <9% for the A647 and <13% for A680.

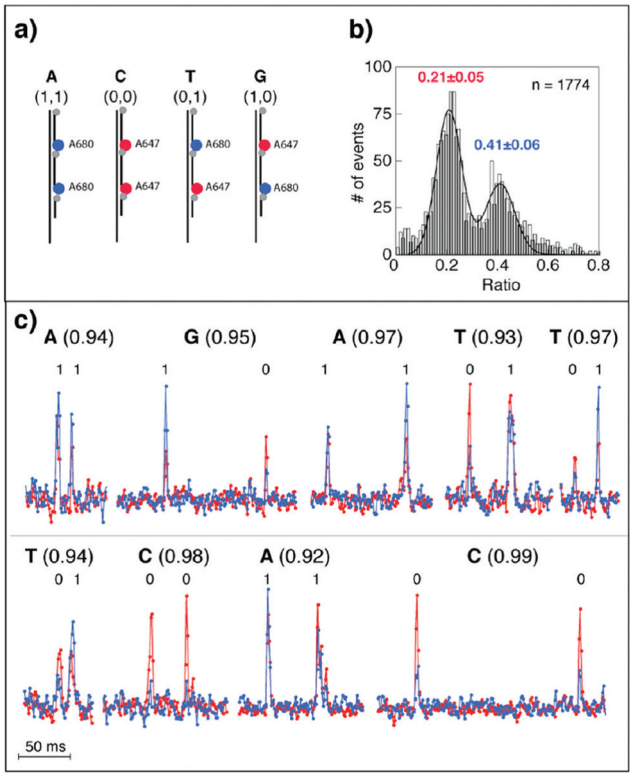

Fig. 10 Optical detection of the four 2-bit combinations representing the four different nucleotides. (a) Illustration of the four samples labeled with two fluorophores correspond to the four bases. (b) The color ratio (*R*) distribution of 1774 events revealing two peaks corresponding to the two fluorophores. (c) Representative intensity corrected fluorescence traces of unzipping events. Corresponding bit called, base called, and certainty score indicated above the event. The intensities in the two channels were corrected automatically by a computer code after each bit is called using a fixed threshold *R* value. Adapted with permission from McNally *et al.*[16] Copyright 2010 American Chemical Society.

Using the calibration results, they tested their ability to discriminate between the 2 bit combinations representing the four different bases (Fig. 10). Analysis of ~2000 events in which two distinct photon bursts were detected revealed a bimodal distribution of R with two modes at 0.21 ± 0.05 and 0.41 ± 0.06, in agreement with the calibration results. Photon bursts with $R < 0.3$ were classified as 0 and those with $R > 0.3$ were classified as 1. Finally, they demonstrated multi-pore reading of the photon bursts using an array of 3 nanopores.

Although this method provides a new approach for high-throughput DNA sequencing, the SNR and error in barcode determination due to spectra overlap must be further improved. One of the possible ways in which the barcoding error can be reduced is by use of fluorophores with less overlap in their emission spectra. This could be achieved by simultaneously illuminating the nanopore with multiple laser lines. Using this idea, Assad and coworkers have been able to extend the range of usable fluorophores, by exploiting low PL nanopores fabricated in a thinned down silicon nitride mem-

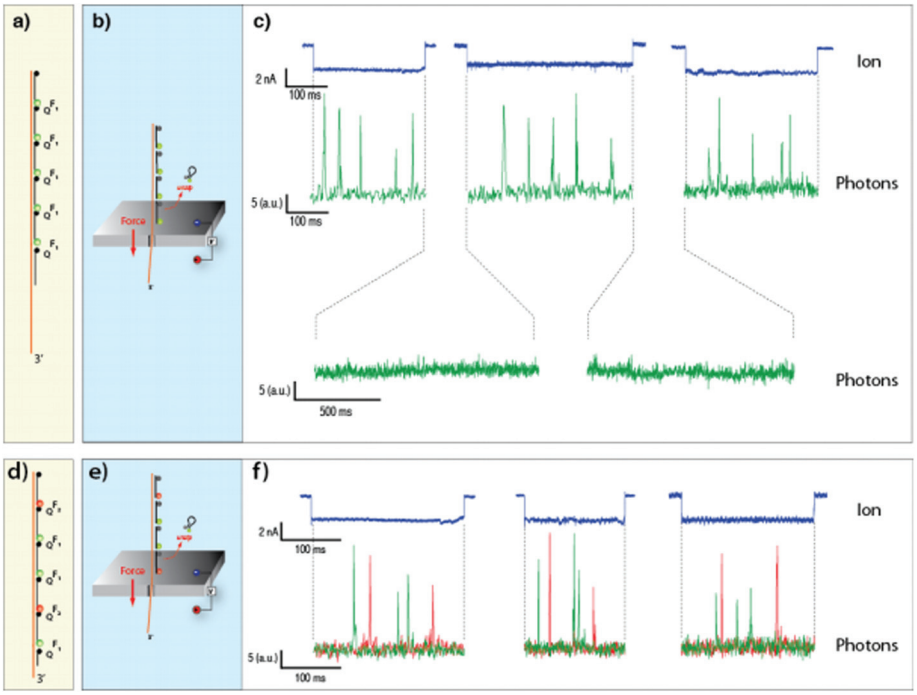

Fig. 11 Single and dual color barcode detection using low PL nanopore. (a,d) Illustration of the ssDNA template consisting 16-mer binding sequences hybridized to molecular fluorophore-quencher labeled beacons. Each DNA strand is labeled with either five green ("F1") fluorophores (a) or specific sequence of green and red ("F1" and "F2", respectively) fluorophores (d) as well as a quencher oligo. The strands are threaded through a low PL, 3 nm nanopores. The marked beacons are stripped off one at the time creating a distinct fluorescent burst (b,e). The electrical and optical signals are measured simultaneously, showing five clear photon bursts per event in the green channel (c) or green and red channels (f) according to the sample. Adapted with permission from Assad *et al.*[47] Copyright 2014 American Chemical Society.

brane. Under these conditions, it was possible to detect DNA labeled with individual green-yellow (5-carboxytetramethylrhodamine, TMR) and red (Atto647) fluorophores having λ_{EM} = 565 nm and 665 nm, respectively.[47] In this study, DNA barcode constructs consisting of five 16-nucleotide-long, fluorophore-quencher beacons hybridized in a head-to-tail configuration along a template strand were used. Assad and coworkers used two alternative constructs: a single-color barcode (TMR), and a dual-color barcode (TMR and Atto647, at a specific order) simultaneously excited by red and green lasers. They simultaneously recorded the electrical current and the optical current; for the optical signals, they used confocal microscopy and 2 APDs, in a configuration similar to that used by Anderson *et al.*[53] The optic events showed five discrete photon bursts associated with the unzipping and fast diffusion of the five molecular beacons hybridized to the template DNA molecule (Fig. 11). In both signals (using a single-color barcode and a dual-color barcode), the SNR was high, and no photon bursts were observed between events.

The ability to use blue and green laser excitations, which was previously impossible due to low SNR, and the new understanding of the nature of PL in SiN_x membranes, may significantly contribute to the improvement of nanopore-based, optical DNA sequencing methods as well as to other future applications.

6. Future advancements

Single-molecule fluorescence sensing has been evolving substantially in the past two decades, opening up new avenues in biomedical research and in biotechnology.[69] Single-molecule, optical sensing in solid-state nanopores is a powerful new approach that allows a high-bandwidth and high-throughput detection from multiple nanopores simultaneously. In this review we focused on the strategies employed to advance optical sensing in small nanopores; namely reduction in the background noise either by optical means to eliminate light emitted by nearby objects or by suppression of photoluminescence originating at the membrane itself. We also described two strategies to enhance the localization of the fluorescence signal to the close vicinity of the nanopore, by introducing a steep gradient of Ca_2^+ ions near the pore, or by the use of molecular beacons that can quench fluorescence from all molecules, except the one residing at the pore entrance.

Optical sensing in nanopores complements the electrical sensing in a number of useful ways. For example, multi-color 'bar-coding' of individual molecules can be used to tag specific DNAs and potentially allow precise quantifications of genes or RNA transcripts, at the single-molecule level. Additionally, the photon emission intensity can be coupled to the nanopore

ionic conductance by the use of Ca^{2+} activated dyes, permitting a purely digital sensing of the pore conductance which is less obscured by electrical interferences. Moreover, optical sensing in nanopores can be integrated with nano-channels that are used to efficiently deliver long double-stranded DNA or other biopolymers.[70] Therefore, and particularly with further improvements of the optical SNR in solid-state nanopores, it is likely that additional sensing applications will be realized. Additionally, other optical approaches, such as Förster Resonance Energy Transfer (FRET),[71,72] Fluorescence Correlation Spectroscopy (FCS)[73] and super resolution strategies such as Stimulated Emission Depletion (STED)[74,75] could be used to further enhance the method, providing it with superior spatial and temporal resolutions.

References

1 M. Wanunu, *et al.*, Electrostatic focusing of unlabelled DNA into nanoscale pores using a salt gradient, *Nat. Nanotechnol.*, 2010, **5**(2), 160–165.
2 M. Wanunu, *et al.*, DNA Translocation Governed by Interactions with Solid-State Nanopores, *Biophys. J.*, 2008, **95**(10), 4716–4725.
3 C. Plesa, *et al.*, Fast translocation of proteins through solid state nanopores, *Nano Lett.*, 2013, **13**(2), 658–663.
4 M. Wanunu and A. Meller, Single-molecule analysis of nucleic acids and DNA-protein interactions using nanopores, in *Single-Molecule Techniques: A Laboratory Manual*, ed. P. Selvin and T. J. Ha, Cold Spring Harbor Laboratory Press, Cold Spring Harbor, NY, 2008, pp. 395–420.
5 C. Dekker, Solid-state nanopores, *Nat. Nanotechnol.*, 2007, **2**(4), 209–215.
6 A. J. Storm, *et al.*, Fabrication of solid-state nanopores with single-nanometre precision, *Nat. Mater.*, 2003, **2**(8), 537–540.
7 B. McNally, M. Wanunu and A. Meller, Electromechanical Unzipping of Individual DNA Molecules Using Synthetic Sub-2 nm Pores, *Nano Lett.*, 2008, **8**(10), 3418–3422.
8 M. J. Kim, *et al.*, Rapid Fabrication of Uniformly Sized Nanopores and Nanopore Arrays for Parallel DNA Analysis, *Adv. Mater.*, 2006, **18**(23), 3149–3153.
9 A. Meller, Nanopores: Single-Molecule Sensors of Nucleic Acid–Based Complexes, in *Advances in Chemical Physics*, John Wiley & Sons, Inc., 2012, pp. 251–268.
10 D. H. Stoloff and M. Wanunu, Recent trends in nanopores for biotechnology, *Curr. Opin. Biotechnol.*, 2013, **24**(4), 699–704.
11 D. Branton, *et al.*, The potential and challenges of nanopore sequencing, *Nat. Biotechnol.*, 2008, **26**(10), 1146–1153.
12 J. Clarke, *et al.*, Continuous base identification for single-molecule nanopore DNA sequencing, *Nat. Nanotechnol.*, 2009, **4**(4), 265–270.
13 B. M. Venkatesan and R. Bashir, Nanopore sensors for nucleic acid analysis, *Nat. Nanotechnol.*, 2011, **6**(10), 615–624.
14 E. A. Manrao, *et al.*, Reading DNA at single-nucleotide resolution with a mutant MspA nanopore and phi29 DNA polymerase, *Nat. Biotechnol.*, 2012, **30**(4), 349–353.
15 M. Ayub, *et al.*, Nanopore-based identification of individual nucleotides for direct RNA sequencing, *Nano Lett.*, 2013, **13**(12), 6144–6150.
16 B. McNally, *et al.*, Optical recognition of converted DNA nucleotides for single-molecule DNA sequencing using nanopore arrays, *Nano Lett.*, 2010, **10**(6), 2237–2244.
17 G. V. Soni and A. Meller, Progress toward ultrafast DNA sequencing using solid-state nanopores, *Clin. Chem.*, 2007, **53**(11), 1996–2001.
18 B. M. Venkatesan and R. Bashir, Solid State Nanopores Sensors for Nucluic Acid Analysis, in *Nanopores, Sensing and Foundamental Biological Interactions*, Springer, 2011.
19 T. Z. Butler, J. H. Gundlach and M. A. Troll, Determination of RNA Orientation during Translocation through a Biological Nanopore, *Biophys. J.*, 2006, **90**(1), 190–199.
20 M. Wanunu, *et al.*, Nanopore analysis of individual RNA/antibiotic complexes, *ACS Nano*, 2011, **5**(12), 9345–9353.
21 M. Wanunu, *et al.*, Rapid electronic detection of probe-specific microRNAs using thin nanopore sensors, *Nat. Nanotechnol.*, 2010, **5**(11), 807–814.
22 M. Firnkes, *et al.*, Electrically facilitated translocations of proteins through silicon nitride nanopores: conjoint and competitive action of diffusion, electrophoresis, and electroosmosis, *Nano Lett.*, 2010, **10**(6), 2162–2167.
23 S. W. Kowalczyk, A. R. Hall and C. Dekker, Detection of local protein structures along DNA using solid-state nanopores, *Nano Lett.*, 2010, **10**(1), 324–328.
24 A. Singer, *et al.*, Electronic barcoding of a viral gene at the single-molecule level, *Nano Lett.*, 2012, **12**(3), 1722–1728.
25 A. Singer, *et al.*, Nanopore based sequence specific detection of duplex DNA for genomic profiling, *Nano Lett.*, 2010, **10**(2), 738–742.
26 J. K. Rosenstein, *et al.*, Integrated nanopore sensing platform with sub-microsecond temporal resolution, *Nat. Methods*, 2012, **9**(5), 487–492.
27 J. D. Uram, K. Ke and M. Mayer, Noise and bandwidth of current recordings from submicrometer pores and nanopores, *ACS Nano*, 2008, **2**(5), 857–872.
28 R. M. Smeets, *et al.*, Noise in solid-state nanopores, *Proc. Natl. Acad. Sci. U. S. A.*, 2008, **105**(2), 417–421.
29 R. M. Smeets, N. H. Dekker and C. Dekker, Low-frequency noise in solid-state nanopores, *Nanotechnology*, 2009, **20**(9), 095501.
30 V. Tabard-Cossa, *et al.*, Noise analysis and reduction in solid-state nanopores, *Nanotechnology*, 2007, **18**(30), 305505.
31 R. dela Torre, *et al.*, Fabrication and characterization of solid-state nanopore arrays for high-throughput DNA sequencing, *Nanotechnology*, 2012, **23**(38), 385308.
32 F. Traversi, *et al.*, Detecting the translocation of DNA through a nanopore using graphene nanoribbons, *Nat. Nanotechnol.*, 2013, **8**(12), 939–945.

33 G. F. Schneider, *et al.*, DNA translocation through graphene nanopores, *Nano Lett.*, 2010, **10**(8), 3163–3167.
34 C. A. Merchant, *et al.*, DNA translocation through graphene nanopores, *Nano Lett.*, 2010, **10**(8), 2915–2921.
35 S. Garaj, *et al.*, Graphene as a subnanometre *trans*-electrode membrane, *Nature*, 2010, **467**(7312), 190–193.
36 B. M. Venkatesan, *et al.*, Stacked graphene-Al2O3 nanopore sensors for sensitive detection of DNA and DNA-protein complexes, *ACS Nano*, 2012, **6**(1), 441–450.
37 D. Axelrod, Total internal reflection fluorescence microscopy in cell biology, *Traffic*, 2001, **2**(11), 764–774.
38 K. N. Andersen, *et al.*, Annealing and deposition effects of the chemical composition of silicon-rich nitride, *Appl. Surf. Sci.*, 2005, **243**(1–4), 401–408.
39 G. V. Soni, *et al.*, Synchronous optical and electrical detection of biomolecules traversing through solid-state nanopores, *Rev. Sci. Instrum.*, 2010, **81**(1), 014301.
40 S. Inoué, Foundations of Confocal Scanned Imaging in Light Microscopy, in *Handbook Of Biological Confocal Microscopy*, ed. J. B. Pawley, Springer, US, 2006, pp. 1–19.
41 N. Di Fiori, *et al.*, Optoelectronic control of surface charge and translocation dynamics in solid-state nanopores, *Nat. Nanotechnol.*, 2013, **8**(12), 946–951.
42 P. Chen, *et al.*, Atomic Layer Deposition to Fine-Tune the Surface Properties and Diameters of Fabricated Nanopores, *Nano Lett.*, 2004, **4**(7), 1333–1337.
43 F. Sawafta, *et al.*, Solid-state nanopores and nanopore arrays optimized for optical detection, *Nanoscale*, 2014, **6**(12), 6991–6996.
44 B. W. Ward, J. A. Notte and N. P. Economou, Helium ion microscope: A new tool for nanoscale microscopy and metrology, *J. Vac. Sci. Technol., B*, 2006, **24**(6), 2871–2874.
45 N. M. Park, *et al.*, Quantum confinement in amorphous silicon quantum dots embedded in silicon nitride, *Phys. Rev. Lett.*, 2001, **86**(7), 1355–1357.
46 M. Wang, *et al.*, Photoluminescence of Si-rich silicon nitride: Defect-related states and silicon nanoclusters, *Appl. Phys. Lett.*, 2007, **90**(13), 131903.
47 O. N. Assad, *et al.*, Two color DNA barcode detection in photoluminescence suppressed silicon nitride nanopores, *Nano Lett.*, 2015, **15**(1), 745–752.
48 R. Huang, *et al.*, Strong green-yellow electroluminescence from oxidized amorphous silicon nitride light-emitting devices, *Appl. Phys. Lett.*, 2007, **90**(9), 093515.
49 H. Rui, *et al.*, Oxygen induced strong green light emission from low-temperature grown amorphous silicon nitride films, *Appl. Phys. Lett.*, 2006, **89**(22), 221120.
50 J. Shuai and I. Parker, Optical single-channel recording by imaging Ca2+ flux through individual ion channels: theoretical considerations and limits to resolution, *Cell Calcium*, 2005, **37**(4), 283–299.
51 A. J. Heron, *et al.*, Simultaneous measurement of ionic current and fluorescence from single protein pores, *J. Am. Chem. Soc.*, 2009, **131**(5), 1652–1653.
52 A. Ivankin, *et al.*, Label-Free Optical Detection of Biomolecular Translocation through Nanopore Arrays, *ACS Nano*, 2014, **8**(10), 10774–10781.
53 B. N. Anderson, *et al.*, Probing solid-state nanopores with light for the detection of unlabeled analytes, *ACS Nano*, 2014, **8**(11), 11836–11845.
54 B. N. Anderson, *Enhancing the Temporal and Spatial Resolution of Solid-State Nanopore Single-Molecule Sensors*, Ph.D. Dissertation, Boston University, Boston, MA, 2013.
55 G. M. Cherf, *et al.*, Automated forward and reverse ratcheting of DNA in a nanopore at 5-A precision, *Nat. Biotechnol.*, 2012, **30**(4), 344–348.
56 Y. Chen, *et al.*, Electroosmotic flow in nanotubes with high surface charge densities, *Nano Lett.*, 2008, **8**(1), 42–48.
57 D. G. Howitt, *et al.*, The electron beam hole drilling of silicon nitride thin films, *J. Appl. Phys.*, 2008, **103**(2), 024310.
58 M. Y. Wu, *et al.*, Control of shape and material composition of solid-state nanopores, *Nano Lett.*, 2009, **9**(1), 479–484.
59 U. F. Keyser, *et al.*, Nanopore tomography of a laser focus, *Nano Lett.*, 2005, **5**(11), 2253–2256.
60 M. P. Jonsson and C. Dekker, Plasmonic nanopore for electrical profiling of optical intensity landscapes, *Nano Lett.*, 2013, **13**(3), 1029–1033.
61 A. Meller and D. Branton, Single molecule measurements of DNA transport through a nanopore, *Electrophoresis*, 2002, **23**(16), 2583–2591.
62 F. Nicoli, *et al.*, DNA Translocations through Solid-State Plasmonic Nanopores, *Nano Lett.*, 2014, **14**(12), 6917–6925.
63 S. Duhr and D. Braun, Why molecules move along a temperature gradient, *Proc. Natl. Acad. Sci. U. S. A.*, 2006, **103**(52), 19678–19682.
64 S. A. Putnam and D. G. Cahill, Transport of nanoscale latex spheres in a temperature gradient, *Langmuir*, 2005, **21**(12), 5317–5323.
65 P. K. Gupta, Single-molecule DNA sequencing technologies for future genomics research, *Trends Biotechnol.*, 2008, **26**(11), 602–611.
66 F. Haque, *et al.*, Solid-State and Biological Nanopore for Real-Time Sensing of Single Chemical and Sequencing of DNA, *Nano Today*, 2013, **8**(1), 56–74.
67 J. Comer and A. Aksimentiev, Predicting the DNA Sequence Dependence of Nanopore Ion Current Using Atomic-Resolution Brownian Dynamics, *J. Phys. Chem. C*, 2012, **116**(5), 3376–3393.
68 W. Timp, J. Comer and A. Aksimentiev, DNA Base-Calling from a Nanopore Using a Viterbi Algorithm, *Biophys. J.*, 2012, **102**(10), L37–L39.
69 C. Joo, *et al.*, Advances in single-molecule fluorescence methods for molecular biology, *Annu. Rev. Biochem.*, 2008, **77**, 51–76.
70 S. Liu, *et al.*, Electro-optical detection of single lambda-DNA, *Chem. Commun.*, 2015, **51**(11), 2084–2087.
71 R. Roy, S. Hohng and T. Ha, A practical guide to single-molecule FRET, *Nat. Methods*, 2008, **5**(6), 507–516.

72 T. Ha, Single-Molecule Fluorescence Resonance Energy Transfer, *Methods*, 2001, **25**(1), 78–86.
73 O. K. a. Bonnet, Fluorescence correlation spectroscopy: the technique and its applications, *Rep. Prog. Phys.*, 2002, **65**, 251–297.
74 S. W. Hell, Far-field optical nanoscopy, *Science*, 2007, **316**(5828), 1153–1158.
75 T. A. Klar, *et al.*, Fluorescence microscopy with diffraction resolution barrier broken by stimulated emission, *Proc. Natl. Acad. Sci. U. S. A.*, 2000, **97**(15), 8206–8210.